Nanoscale

Mapping the thermal entrenchment behavior of Pd nanoparticles on planar SiO2 supports

Journal:	*Nanoscale*
Manuscript ID	NR-ART-04-2020-002941.R1
Article Type:	Paper
Date Submitted by the Author:	21-Jun-2020
Complete List of Authors:	Gosavi, Abha; Northwestern University, Chemical and Biological Engineering Mirkin, Chad; Northwestern University, Chemistry Notestein, Justin; Northwestern University, Chemical and Biological Engineering

Mapping the thermal entrenchment behavior of Pd nanoparticles on planar SiO_2 supports

Abha Gosavi[#, ‡], Chad Mirkin[#, ‡, §, ψ, *], Justin Notestein[#, *]

[#]Department of Chemical and Biological Engineering, [‡]International Institute for Nanotechnology, [§]Department of Chemistry, and [ψ]Department of Materials Science and Engineering, Northwestern University, 2145 Sheridan Road, Evanston, Illinois 60208, United States

**chadnano@northwestern.edu, j-notestein@northwestern.edu*

Abstract

Thermal treatment of metal nanoparticles at temperatures above 1000 ºC lead to the formation of nanopores in amorphous SiO_2 planar supports. In this work, we employ Pd/SiO_2 as a model system to investigate how the initial size and distribution of nanoparticles on the SiO_2 surface affects the behavior of the nanoparticles at high temperatures with respect to the formation of nanopores and related structures. We also examine the role of physical processing parameters such as heating temperature, ramp rate, and heating time in altering the type, size, and number density of features formed. These studies reveal that nanopore formation competes with other surface phenomena, including nanoparticle agglomeration and encapsulation, which also occur at high temperatures. We establish that the dominant behavior, among the many competing phenomena occurring at the metal-oxide interface, depends on the initial surface distribution of the nanoparticles. Using this knowledge, we show that the final nanopore diameter and surface density are highly tunable.

1. Introduction

Metal-oxide and metal-metal interactions, especially at high temperatures, are of critical importance in catalysis[1–4] and electronics.[5,6] The metal-oxide interface is a catalytically active site for many industrially important reactions. At high temperatures, catalyst deactivation can occur via sintering or encapsulation due to surface rearrangement at the metal-oxide interface.[7–11] Similarly, thin films of metals deposited on oxide layers are used for the fabrication of electronic devices where the metal-semiconductor interface is of significance.[12,13] At high temperatures, the stability of these films is reduced by dewetting.[14–17] Thus, the understanding of metal-oxide interactions at high temperatures is important for designing stable catalysts and electronic devices. To this end, these interactions have been studied for a wide range of metals (Au, Pd, Pt, Cu) and oxides (TiO_2, SiO_2, Al_2O_3) across different temperature ranges.[7–9,12,13,18–24] At elevated temperatures (above 600 ºC) metal-oxide interactions, especially for metal nanoparticles, lead to a wide range of behaviors including agglomeration,[7,25] Ostwald ripening,[7,20] diffusion,[26,27] reaction,[11,28] encapsulation,[9,18] and in some instances, nanopore formation.[29–32] In this work, we demonstrate that, at conditions where multiple phenomena are kinetically favored, the extent to which each of these will occur depends upon the size and surface density of the metal nanoparticles as well as the thermal conditions employed.

Nanopore formation, predominantly observed for metal nanoparticles on amorphous SiO_2, occurs at very high temperatures (>1000 ºC).[29–32] This behavior is also described here as nanoparticle entrenchment since, in some cases, metal nanoparticles have been shown to persist at the bottom of the pores.[31] Nanopores and embedded

nanoparticles formed in this manner can be used in separations, catalysis, and electronics.[29,33–35] In this work, we employ Pd nanoparticles supported on planar SiO_2 as a model system to study nanopore formation and entrenchment behavior as a function of different heating conditions (temperature, time, and ramp rate) and initial surface distributions (nanoparticle size and surface density). Of all the metals that have exhibited nanopore formation (Au, Ag, Cu, Pd, and Pt), Pd nanoparticles entrench the most rapidly (within 10 minutes of heating) and tend to form linear nanopores thus making them ideal candidates for a study of this kind.[29] Planar SiO_2 was used rather than high surface area silica particles to avoid interference from pre-existing surface porosity on high surface area particles and to gain additional insights by using techniques like atomic force microscopy (AFM) to reimage the same spot after chemical and thermal different treatments. In general, the Pd/SiO_2 system has been thoroughly studied for different behaviors at high temperatures due to its relevance to the field of catalysis.[19,36–38] Additionally, the low solubility of Pd in the SiO_2 matrix[27] minimizes potential Pd loss by diffusion into SiO_2.

In our previous work, we proposed a mechanism for nanopore formation that is observed when metal nanoparticles supported on amorphous SiO_2 are heated to temperatures above 1000 ºC. At high temperatures (above 900 ºC), the solubility of metals in the SiO_2 matrix is significant, and when the metal atoms diffuse into SiO_2, they lower its glass transition temperature (T_g). At temperatures above the T_g (~1000 ºC), SiO_2 exhibits viscoelastic behavior, allowing the nanoparticles to form nanopores.[29] It has also been proposed that the slow evaporation of the metal nanoparticles at the surface causes the continuous renewal of the metal-SiO_2-vapor interface and prevents the total

encapsulation of the metal nanoparticle within the SiO_2 matrix.[31] In the case of Au nanoparticles, the Au (111) plane of the nanoparticle is expected to not melt, which pins the nanopore and prevents its closing/pinching.[31]

When metal nanoparticles entrench within the SiO_2 surface at high temperatures, they form nanopores that could extend through the entire thickness of the SiO_2 layer. We previously showed that nanopore formation occurs only above a certain minimum temperature (1000 ºC for Au nanoparticles).[29] Additionally, the nanoparticles, depending on their composition and size, require different temperatures and heating times to entrench.[29] The resulting nanopores are characterized by two features: its pore diameter and the height of its oxide ridge. The oxide ridge surrounding the nanopore is formed as a result of oxide transport occurring due to the shifting surface energy equilibrium at the metal-oxide-gas triple line.[17,31] Understanding how phenomena such as agglomeration, diffusion, and encapsulation, also occurring at these high temperatures, compete with nanopore and oxide ridge formation will provide a fundamental understanding of the metal-oxide interactions that lead to nanopore formation. Moreover, this will also help define synthesis conditions for nanopores of desired dimensions. Here, we first examine Pd nanoparticles with different initial sizes (1.5 – 25 nm) and surface densities (5 – 7000 nanoparticles/μm^2) and establish how the initial surface distribution of the nanoparticles defines the final size and surface density of the nanopores.

To understand the role of thermal processing in nanopore formation, several representative initial distributions of the Pd/SiO_2 system were further studied under different heating conditions (temperature, hold time, and ramp rate). The features observed after heating include nanopores, partially embedded nanoparticles,

agglomerated nanoparticles without nanopore formation, and nanoparticles encapsulated in SiO_2. We observe that the types of surface features present after heating depend on the initial size and surface density of the nanoparticles. We also show that tuning the initial size and surface density of Pd nanoparticles on SiO_2 controls the nanopore diameter and height of the surrounding oxide ridge. The interplay of agglomeration and nanopore formation limits the maximum surface density of nanopores to ~150 nanopores/$\mu m^{2,}$ but a range of nanopore sizes (5 - 25 nm) are observed depending on the initial particle size distribution.

2. Methods

a. Nanoparticle synthesis

Randomly distributed Pd nanoparticles on SiO_2 surfaces were synthesized using block copolymer micelle lithography.[39–41] Aqueous solutions of Pd-containing micelles were synthesized by combining the diblock copolymer, polyethylene oxide-b-polyvinyl pyridine (PEO-*b*-P2VP) of varying chain lengths (Table S1,Polymer Source, Inc.) and Na_2PdCl_4 at different pyridyl: Pd molar ratios (32:1, 16:1, 8:1, 4:1, 2:1, 1:1, and 0.5:1) and shaking overnight. The solution pH was maintained between 3-4 by adding dilute HCl. Thin films of the Pd-containing micelle solution were spin-cast on Si wafers (NOVA Electronic Materials, 285 nm thermal oxide) at different rotation speeds (1000 RPM, 2000 RPM, 3000 RPM, and 4000 RPM). Some of the samples were treated with oxygen plasma for different intervals (1 min, 2 min, 3min, and 5 min) (Plasma Etch Inc., PE 50XL, 30 W) to control the surface densities of Pd nanoparticles. The Pd-containing micelles were then reduced to nanoparticles by thermal annealing in a tube furnace (ThermoScientific Blue) under flowing argon gas (195 sccm; ramp 4 ºC/min to 150 ºC, hold for 10 h) and then

flowing H_2 gas (195 sccm; ramp 11 ºC/min to 500 ºC, hold for 10 h). The resulting Pd nanoparticles (Pd/SiO_2) have sizes ranging from 1.5 - 25 nm and surface densities from 5 - 7000 nanoparticles/μm^2. A detailed description of the initial Pd nanoparticle sizes and distributions resulting from different synthesis conditions is included in the supplementary materials and illustrated in Figure S1.

b. Rapid thermal processing (RTP)

Heating of the Pd/SiO_2 was performed under flowing Ar (100 sccm) in a rapid thermal processing (RTP) furnace (MTI Corporation, OTF-1200X-4-RTP-UL). Most samples were treated at 1040 ºC for 10 min using a ramp rate of 3.3 ºC/s from room temperature. However, ramp rates were varied between 0.33 and 3.3 ºC/s, hold temperatures between 850 and 1040 ºC, and hold times between 1.5 and 20 min. The samples were passively cooled to room temperature under flowing Ar (25 sccm). The furnace cooled from ~1000 ºC down to 480 ºC in less than 5 min, while 480 ºC to room temperature took ~ 2 h.

c. Surface features and composition characterization

Atomic force microscopy (AFM) was performed on a FastScan (Bruker) using FastScan C probes. AFM image analysis and quantitative measurements were performed using the Nanoscope Analysis software (Bruker). For increased accuracy in scanning the same sample at different stages of synthesis and thermal treatment, a light scratch mark was made with a diamond pen and AFM imaging was performed at a known distance from the mark. For the nanoparticle distributions with a low surface density of nanoparticles, the nanoparticle height and radius are comparable and remain fairly unchanged at elevated temperatures. In these cases, the nanoparticle heights reported by the software are

defined as the standard nanoparticle size since the nanoparticle diameters detected by the AFM could be erroneous due to tip convolution effects.[42] However, for nanoparticle distributions that have a very high surface density, particle coalescence occurs at elevated temperatures.[7] In these cases, the agglomerated nanoparticles form islands that have very disparate diameters and heights. For such distributions, nanoparticle diameters are considered as the standard size. Nanopore diameters are defined as the standard nanopore size since the depth of the nanopore cannot be determined accurately using AFM.

The Pd nanoparticle surface coverage is defined as the percent of the SiO_2 surface in contact with the Pd nanoparticles. AFM images are processed in the software Image J, and a Pd-SiO_2 contact angle of 90º or less is assumed. The Pd/SiO_2 surface composition was analyzed before and after RTP using X-ray photo-electron spectroscopy (XPS) equipped with an Al-source with a spot size of 500 μm (ThermoScientific, Escalab 250 Xi). To study the surface profile of the oxide ridges around partially embedded Pd nanoparticles, the surfaces were etched using a Pd etchant solution (Transene) before imaging the surface via AFM.

3. Results and Discussion

a. Different behaviors observed at high temperatures

After subjecting the library of Pd/SiO_2 surfaces to rapid thermal processing (RTP) consisting of a ramp to 1040 ºC at rate 3.3 ºC/s followed by a hold at that temperature for 10 min, we observe different surface features. For most initial Pd nanoparticle distributions, a variety of surface features showing Pd nanoparticles in various stages of entrenchment are observed (Figure 1). For a representative distribution, we observe that

the nanoparticles agglomerate before they entrench. This is apparent because the initial surface has ~600 nanoparticles/μm^2 with an average height of 6.5 nm ± 2.8 nm, while the final distribution after RTP has ~60 features/μm^2, including both nanopores and nanoparticles in various stages of entrenchment (Figure 1A and B). The commonly observed surface features include agglomerated (but not entrenched nanoparticles), partially and near-completely entrenched nanoparticles, and nanopores (Figure 1C). Each of these features is accompanied by oxide ridge formation around both the nanoparticles and nanopores. Additionally, we also observe positive surface features that cannot be removed by metal etching, which indicate the encapsulation of the Pd nanoparticles by SiO_2 that has become mobile at these temperatures. To quantify these different behaviors, we define two non-dimensional parameters: pore fraction (f_{Pore}) and extent of agglomeration (E_{Agg}) (Equations 1 and 2, respectively).

$$f_{Pore} = 100 \times \left(\frac{Number\ of\ nanopores\ /\ \mu m^2}{Total\ number\ of\ features\ (nanopores + nanoparticles)\ /\ \mu m^2} \right)$$

$$E_{Agg} = 100 \times \left(1 - \frac{Final\ number\ of\ features (nanopores + nanoparticles)\ \ per\ \mu m^2}{Initial\ number\ of\ nanoparticles\ per\ \mu m^2} \right)$$

For very small nanoparticles with low surface densities (size < 2 nm, surface density < 150 nanoparticles/μm^2), the surface features after RTP become indistinguishable from the surface roughness (± 1 nm) of the SiO_2 layer (Figure S2). The nanoparticles may either be diffusing into the substrate[27] or evaporating.[43] On the other hand, RTP of large nanoparticles with high surface densities (size ~ 7 nm, surface density ~ 4000 nanoparticles/μm^2) such that the nanoparticles form multilayers, results in overlapping nanopores in the SiO_2 substrate (Figure S3). These two extreme distributions are excluded from consideration. In the majority of other cases, the final surface features

are readily counted and characterized. In these cases, decreases in the number density of the features (E_{Agg} > 0) are accompanied by increases in the size of the remaining features. For cases where no nanopores form, the total volume of the Pd-containing surface features is approximately conserved after RTP (Table S2), confirming that agglomeration of small particles into larger ones is the primary pathway for loss of surface feature number density.

The surface speciation after RTP (hold at 1040 ºC for 10 min and a ramp rate of 3.3 ºC/s) is shown in Figure 2A as a function of different initial surface distributions. As discussed above, four different behaviors were identified and quantified across the entire range: 1) complete entrenchment, 2) partial entrenchment, 3) agglomeration (with no entrenchment during the heating time allotted), and 4) encapsulation. The different ranges of E_{Agg} and f_{Pore} used to define these behaviors are illustrated in Figure 2B. These behaviors are observed across the entire range of initial nanoparticle size and surface densities considered (Figure S5).

Since we previously showed the RTP of metal nanoparticles at temperatures such as employed here produce nanopores, it is not surprising that complete nanoparticle entrenchment (f_{Pore} > 75% and 0 < E_{Agg} < 100%) is the most frequently observed outcome.[29,31] Complete entrenchment is accompanied by the formation of oxide ridges around the nanopores. Even though the nanopore depth cannot be quantified using AFM due to tip-size limitations, we have previously employed cross-sectional electron microscopy to show that under these RTP conditions, most nanopores extend the entire thickness of the SiO_2 layer (285 nm in this case).[29] In addition to complete entrenchment, partial entrenchment (10% < f_{Pore} < 75% and 0 < E_{Agg} < 100%) is also observed. In these

cases, some nanoparticles form nanopores, while others only partially entrench or do not entrench to an observable extent during the heating time. The third behavior, agglomeration (not accompanied by nanopore formation; 10% < f_{Pore} and E_{Agg} > 10%) is characterized by a reduction in the nanoparticle surface density and a corresponding increase in nanoparticle height, without any apparent entrenchment. This presumably occurs when lateral mobility on the surface is favored over entrenchment within the annealing time (10 min). However, after longer annealing, both the partially entrenched and agglomerated nanoparticles result in nanopore formation (Figure S6). This indicates that the rate of nanopore formation in these cases is slowed, but not prohibited. However, for some initial nanoparticle distributions, neither nanopore formation nor agglomeration are observed (f_{Pore} < 10% and E_{Agg} < 10%), even after extended heating. As discussed below, these features are characterized as Pd nanoparticles that have been encapsulated by SiO_2.

Examining the data in aggregate, several conclusions can be made. First, nanopore formation, with partial or complete entrenchment, occurs across almost the entire range of initial nanoparticle sizes and surface densities (Figure S4). Second, Pd surface coverages appear to be critical. Coverages above 20% always result in agglomeration, with or without nanopore formation (Figure 3), whereas coverages below 20% rarely agglomerate before entrenchment. Surface area coverage is a function of both the nanoparticle size and surface density such that large nanoparticles with low surface density (e.g. 12 nm and 80 nanoparticles/μm^2) have the same surface area coverage (8.5%) as that of small nanoparticles with high surface density (e.g. 3 nm and 750 nanoparticles/μm^2). Low coverages and higher surface densities favor agglomeration

before nanopore formation. The two parameters can generally predict the dominant behavior upon RTP (complete entrenchment, partial entrenchment, agglomeration, or encapsulation).

Surfaces of particular interest from the perspective of materials design are those for which the sizes and surface densities of the final features are very similar to the initial nanoparticles availing a greater predictability and control. For this purpose, E_{agg} < 20% is desirable. These all have nanoparticle surface coverages < 20% (Figure 4), specifically, initial nanoparticle distributions of 4 - 25 nm and 5 - 450 nanoparticles/μm^2. These surface densities correspond to interparticle spacings of 30 - 60 nm, which appear to be large enough to minimize agglomeration. Within this region, < 5% Pd surface coverage (i.e. 6 - 25 nm nanoparticles and 5 – 350 nanoparticles/μm^2) primarily results in complete or partial entrenchment after 10 min at these RTP conditions, as the nanoparticles are large enough to resist encapsulation (Figure 4B). In contrast, nanoparticle encapsulation is observed at 5 – 15% surface coverage (i.e. smaller 4 – 8 nm nanoparticles with 250 – 450 nanoparticles/μm^2) (Figure 4A). Thus, in the absence of agglomeration, the entrenchment (complete or partial) and encapsulation are the two dominant behaviors and occur over mutually exclusive ranges of initial nanoparticle distributions. No attempt is made to identify distributions that favor complete entrenchment over partial entrenchment, since the latter can be eliminated by continued heating.

Overall, these considerations allow us to predict the dominant behaviors for various sizes and surface densities after RTP. We expect larger nanoparticles (10 - 25 nm) with low surface densities (< 200 nanoparticles/μm^2) to form nanopores without agglomeration. Similarly, smaller (1 - 10 nm) nanoparticles with high surface densities

(100 - 7000 nanoparticles/μm^2) are highly mobile and will agglomerate before entrenchment. Nanoparticles with distributions between these two extremes (4 - 8 nm nanoparticles and 250 - 450 nanoparticles /μm^2) will be encapsulated within the SiO_2 support.

b. Understanding encapsulating behavior

While most nanoparticle distributions studied here ultimately lead to nanopore formation, we noted above that some nanoparticle distributions remain unchanged after RTP, with no apparent nanopore formation (Figure 5A i-ii). Additionally, the surface features do not undergo further transformation upon extended heating, unlike the partially entrenched or agglomerated nanoparticles (Figure 5A iii). Furthermore, the surface features remaining after RTP have approximately the same size, number density, and spatial arrangement as the initial Pd nanoparticles (Figure S8). However, for these samples, the Pd XPS signals are lost after RTP (Figure 5B). The conclusion most consistent with all these observations is that the Pd nanoparticles are encapsulated by a layer of SiO_2, which acts as barrier to entrenchment.

It has been reported that strong metal-surface interactions (SMSI) lead to encapsulation of metal nanoparticles in reducible oxides.[8,10,18] To investigate if certain distributions of Pd nanoparticles become encapsulated by SiO_2, samples were treated with a Pd etchant following RTP. For the nanoparticle distributions where no apparent change was observed after RTP, the surface topology also remained unchanged after the Pd etch (Figure 5A iv) indicating that some protective layer, assumed to be SiO_2, exists over the features. In cases where the Pd nanoparticles were partially embedded in the support, Pd etching reveals only the oxide ridges formed around the nanoparticles (Figure

S7). The SMSI effect is typically reported to be almost negligible for Pd/SiO_2,[9] in contrast it is strong for Pd on other reducible oxides (e.g. Al_2O_3 or TiO_2). However, most studies are carried out far below 1000 ºC. Under RTP conditions, Pd diffuses into the SiO_2 and causes the support to become viscoelastic.[29] At this point, the SiO_2 is sufficiently mobile to fully encapsulate the nanoparticles during oxide ridge formation (Scheme 1A). It is also possible that the nanoparticles do entrench, but that the oxide ridges are sufficiently large to close off the nanopore (Scheme 1B). In each scenario, neither the nanoparticle nor the nanopore are accessible, effectively resulting in nanoparticle encapsulation.

c. Entrenchment at different heating conditions

Previously, we reported that 10 - 15 nm Au nanoparticles required temperatures > 1000 ºC and hold times > 10 min to form nanopores in SiO_2,[29] but Ag nanoparticles of the same size entrenched at ~900 ºC. In the previous sections, we saw that the nature of entrenchment depends on the initial nanoparticle distribution and the competition between nanopore formation and other surface phenomena. In this section, we report on the evolution of nanopores under different RTP conditions (annealing time, temperature, and ramp rates) for two characteristic Pd/SiO_2 distributions: one with E_{Agg} < 20% (large particles and low surface density) and another with E_{Agg} > 80% (small particles and high surface density; see Figure S9).

(i) Effect of Hold Temperature

Two distributions of Pd/SiO_2 were studied following RTP (10 min hold times and ramp rates of 3.3 ºC/s) using hold temperatures between 850 ºC and 1040 ºC. For a high surface density of small nanoparticles (3 - 4 nm and > 5000 nanoparticles/μm^2), only agglomeration is observed at 850 and 900 ºC. Here, the nanoparticle surface density

297 decreases from > 5000 to ~ 2000 nanoparticles/μm^2 and the nanoparticle size increases
298 from ~ 3.5 to 6 nm after RTP (Figure 6). RTP at 950 ºC shows further agglomeration such
299 that the nanoparticle surface density decreases to 60 nanoparticles/μm^2 while the
300 nanoparticle size increases five-fold. At hold temperatures of 1000 and 1040 ºC, the
301 agglomerated nanoparticles entrench into the SiO_2 surface, resulting in nanopores with
302 diameters similar to the size of the agglomerated nanoparticles (Fig. 5B).

303 The behavior of Pd/SiO_2 with fewer, larger nanoparticles (6 - 7 nm and surface
304 densities of ~200 nanoparticles/μm^2) is significantly different (Figure 7). Since these
305 nanoparticles have larger interparticle spacings, agglomeration is not as common, and
306 the size and surface densities remain approximately constant after RTP at 850 ºC and
307 900 ºC. After 10 min at 950 ºC, nanoparticle size and density do not significantly change,
308 but oxide ridge formation is observed around the Pd nanoparticles without complete
309 entrenchment. This behavior is similar to what we previously reported for Au
310 nanoparticles of similar sizes and surface densities following RTP at 900 ºC.[29] For this
311 Pd/SiO_2 distribution, nanopore formation begins at 1000 ºC, although < 20% of the
312 nanoparticles initially entrench. By 1040 ºC nearly all nanoparticles form nanopores, and
313 the average diameter of the resulting nanopores is comparable to the initial nanoparticle
314 size. This case demonstrates that agglomeration to a certain size is not a prerequisite for
315 nanopore formation in cases where agglomeration isn't kinetically favored. Indeed, of the
316 two cases compared here, the initially smaller nanoparticles first agglomerate and then
317 form larger nanopores (Scheme 2A), while the initially larger, well-spaced nanoparticles
318 are fairly immobile and do not transform until subjected to entrenchment temperatures
319 (Scheme 2B), ultimately resulting in smaller nanopore diameters. For both distributions,

oxide ridge formation is observed at temperatures slightly below the onset of entrenchment. Overall, agglomeration and entrenchment/nanopore formation are all kinetically driven behaviors, and they depend on both temperature and initial nanoparticle size. The kinetic activation barrier to entrenchment appears to be higher than those for agglomeration and oxide ridge formation, thus explaining its dominance at the highest temperatures.

(ii) Effect of Hold Time

The same two surface distributions of Pd/SiO_2 were studied to determine the effect of hold time, following RTP with a ramp rate of 3.3 ºC/s and a hold temperature of 1040 ºC. For a high surface density of small nanoparticles, only agglomeration is observed during the first 1.5 min (Figure 8). After 3 min, agglomeration remains dominant, but some nanopores begin to form, and oxide ridges are observed around the nanoparticles. Between 3 and 5 min, all the agglomerated nanoparticles entrench forming nanopores whose average diameter and density is similar to that of the agglomerated nanoparticles. While the nanopore depth cannot be determined using AFM, it was seen that the nanoparticles have entrenched beyond the range of the tip. These observations prove that, when both occur, entrenchment and agglomeration are sequential processes. At the highest temperatures, small and highly mobile nanoparticles have high rates of agglomeration. Once they grow to a certain size, the relative rate of entrenchment increases, and nanopore formation starts. In contrast, for initially larger nanoparticles and lower surface densities, agglomeration does not readily occur, instead nanopores form in the first 1.5 min of RTP to 1040 ºC with no other competing surface phenomena (Figure 9).

(iii) Effect of Ramp Rates

In addition to the RTP hold temperature and time, the temperature ramp rate influences the nature of the resulting surface features. For both Pd/SiO_2 distributions tested, a ramp rate of 0.33 ºC/s to 1040 ºC combined with a 10 min hold results in only agglomeration and encapsulation with no distinct nanopores (Figure 10A i and B i). At ramp rate of 1 ºC/s however, small nanoparticles at high surface density undergo complete nanopore formation (Figure 10A ii), while the larger nanoparticles at low surface density undergo distinct oxide ridge formation, but only partial entrenchment (Figure 10B ii). Complete entrenchment is observed for both the nanoparticle distributions at a ramp rate of 3.3 ºC/s.

In previous sections, we showed that agglomeration is dominant until 900 ºC, oxide ridge formation occurs at 950 ºC, and nanopore formation starts at 1000 ºC. With ramp rates < 1 ºC/s, the nanoparticles stay at temperatures favoring agglomeration and oxide ridge formation for longer periods. In this situation, they may become encapsulated by tall oxide ridges resulting from continuous oxide transport at the interface, and no distinct nanopores are formed by the time they attain entrenchment temperatures. On the other hand, ramp rates of 3.3 or 10 ºC/s (Figure S10) minimize the residence time below 1000 ºC and ensure distinct pore formation. It is important to note that the slowest ramp rate we used (0.33 ºC/s) is higher than standard ramp rates used in the preparation of catalytic materials (e.g. 0.16 ºC/s or 10 ºC/min) thus explaining why nanopore formation has not been readily observed in literature. Some prior reports have achieved nanopore formation at lower ramp rates, but with initial particles sizes ~1 μm resulting in nanopores of large diameters (200 nm) and comparatively smaller oxide ridges (20 nm).[31] However, in cases

where the height of the oxide ridge is comparable to the nanopore diameter, as considered in this work, large oxide ridges can undesirably close off nanopores or encapsulate the nanoparticles.

d. Nanopore formation on complete entrenchment

The nanopores formed through the method of high temperature entrenchment as demonstrated here, could have a wide range of applications depending on their diameters and aspect ratios. As shown in the proceeding sections, the nanopore diameter and surface density, as well the height of their surrounding oxide ridges, depend strongly on the initial size and surface density of the nanoparticles and their resulting tendency to agglomerate before entrenchment (Figure 11). Figure 11A and B show how the nanopore diameter and the height of the oxide ridge surrounding it change with changing Pd nanoparticle size and surface density on SiO_2. Low surface densities of large nanoparticles do not significantly agglomerate before entrenchment (E_{Agg} < 20%) and form nanopores with diameters and surface densities comparable to their initial distribution. On the contrary, high densities of small nanoparticles undergo significant agglomeration (E_{Agg} > 80%) and eventually form nanopores with larger diameters of 10 - 15 nm and significantly lower surface densities (<200/μm^2) than their initial distribution before rapid thermal processing. This indicates that when agglomeration precedes nanopore formation, the nanoparticles aggregate to a similar size and surface density before entrenchment, irrespective of their initial surface distributions.

We also observe that the oxide ridges are larger when the nanoparticles do not agglomerate, even when they produce comparable nanopore diameters (Figure 11B).

Since small nanoparticles are very mobile on the surface, the metal-oxide-vapor triple-line[44] is also mobile (Scheme 3A). Since the triple-line is the location of ridge formation, individual ridges do not have as much time to grow as when the nanoparticle and triple-line remained fixed (Scheme 3B). Thus, if minimal oxide ridges are desired, it would be preferable to begin with high surface densities of small nanoparticles where agglomeration occurs agglomerate before entrenchment. Different diameters and surface densities may be desired, depending on the application of the nanopores. Table S3 and Figure S11 highlight the different nanopore distributions resulting from certain initial nanoparticle distributions and RTP conditions, as may be useful to the practitioner to design desired surface features.

4. Conclusions

At high temperatures, oxide-supported metal nanoparticles undergo a number of processes including aggregation[7,12] and evaporation,[43] the mechanisms of which have been extensively studied. At the same conditions, restructuring of the oxide surface has also been observed, including encapsulation of the metal nanoparticle[9,18] or the formation of nanopores (entrenchment).[29–32,45,46] In our prior work we showed how entrenchment depends on metal and oxide identity and on the temperature of the thermal treatment, but our and others findings were limited primarily to low particle surface densities (< 100 nanoparticles/μm^2).[29,31,32,45] In contrast, many studies on metal nanoparticle aggregation, e.g. for applications in heterogeneous catalysis, have been carried out at much higher surface densities.[7,47,48] It has not been clear how to reconcile these two extreme behaviors.

In this new study, we have shown that the competition between encapsulation, entrenchment, and aggregation processes depend strongly on Pd nanoparticle surface density and initial size. In particular we have established that small nanoparticles with high surface densities (1-10 nm, 100-7000 nanoparticles/μm^2), will agglomerate before forming nanopores whereas large nanoparticles with low surface density (10-25 nm, < 200 nanoparticles/μm^2), having very low surface mobility, will form nanopores of comparable surface densities. We also report and explain a third behavior- nanoparticle encapsulation. This behavior occurs for nanoparticles that do not have high enough surface densities (250- 450 nanoparticles /μm^2) to favor agglomeration and their small size (4-8 nm) allows for the SMSI between Pd and SiO_2 at high temperatures (above 1000 ºC) to completely encapsulate the nanoparticles.

Having understood the different end behaviors at various sizes and surface densities of Pd nanoparticles on SiO_2 substrates on RTP, we have further studied the dependence of these phenomena on the heating conditions including temperature, time, and ramp rates. We establish that the nanopore formation is kinetically driven and occurs at a certain temperature and time above which increasing temperature and hold time causes a greater extent in entrenchment. Of the two distributions studied here, nanoparticles with smaller particle sizes and high surface densities (1-10 nm, 100-7000 nanoparticles/μm^2), agglomerate first to a size of 20-25 nm and then proceed to form nanopores of comparable sizes. The rate at which the nanoparticles distributions are heated to entrenchment temperatures also plays a crucial role in the final surfaces observed. When Pd nanoparticles are slowly heated to entrenchment temperature (< 1 ºC/s) they have enough time to equilibrate with the supporting oxide and have a greater

tendency to form tall oxide ridges that ultimately encapsulate the nanoparticle or block off any nanopore that may form. However, when higher rates are employed, the nanoparticles reach entrenchment conditions faster, bypassing encapsulation by extensive oxide ridge formation. However, for surfaces where agglomeration is favored, nanoparticles will always proceed through that pathway before entrenchment. We thus establish that although agglomeration and nanopore formation are kinetically driven, oxide ridge formation is thermodynamically driven. For other metallic nanoparticles, we anticipate that while the general trends will hold, as previously shown,[29] the competition between different behaviors at various surface densities and size ranges, will depend on their sintering tendencies[48] and diffusivities in SiO_2.[27]

The nanopores in oxides formed via the RTP of metal nanoparticles may have applications in sensing,[31] separations,[33,34] electronics design,[35] and catalysis.[29,32] In this work, we have demonstrated that the average diameter and surface density of the nanopores can be tuned by controlling the average size and distribution of the initial metal nanoparticles. In general, nanopores of similar diameters can be synthesized from two distinct initial nanoparticle distributions, with or without the intervening agglomeration of the nanoparticles. Nanopores formed from a low surface density of large nanoparticles have tunable pore sizes that are comparable to the initial nanoparticle dimensions. However, these nanopores tend to be accompanied by tall oxide ridges which may not be desirable in some applications (e.g. a nanopore filtration apparatus). Almost ridge-free nanopores can be achieved via RTP of a high surface density of small nanoparticles that first agglomerate and then entrenching producing 10 – 15 nm diameter nanopores. Low surface densities of small nanoparticles can lead to encapsulation and should be avoided

if nanopores are desired. Nanopores fabricated in this way have the advantage of requiring only two steps: metal deposition and RTP, and no additional chemical agents. This is in contrast to traditional templated synthesis techniques,[49] which involve many additional processing steps and potentially costly pore templating agents. The method for nanoparticle synthesis for this purpose is not limited to block copolymer lithography, as shown in this work. A range of different techniques could be employed,[50–52] if the goal were faster and more scalable nanopore synthesis. These findings will help one create designer substrates that could be important in catalysis, molecular separations, and nanoporous device construction. in basically two steps- nanoparticle deposition and RTP, that can be scaled easily.

Acknowledgements

This material is based upon work supported by the Sherman Fairchild Foundation, Inc. and the Air Force Office of Scientific Research under Award number FA9550-16-1-0150. This work made use of the EPIC and SPID facilities of Northwestern University's NUANCE Center, which has received support from the Soft and Hybrid Nanotechnology Experimental (SHyNE) Resource (NSF ECCS-1542205); the MRSEC program (NSF DMR-1121262) at the Materials Research Center; the International Institute for Nanotechnology (IIN); the Keck Foundation; and the State of Illinois, through the IIN.

References

1 P. C. Flynn, *Catal. Rev.*, 1975, **12**, 93–135.

2 P. Wynblatt, *Acta Met.*, 1976, **24**, 1175--1182.

3 S. Schauermann, N. Nilius, S. Shaikhutdinov and H. J. Freund, *Acc. Chem. Res.*, 2013, **46**, 1673–1681.

4 B. Coq, *Coord. Chem. Rev.*, 1998, **180**, 1753–1783.

5 Y. Zhou and S. Ramanathan, *Crit. Rev. Solid State Mater. Sci.*, 2013, **38**, 286–317.

6 B. Dieny and M. Chshiev, *Rev. Mod. Phys.*, , DOI:10.1103/RevModPhys.89.025008.

7 T. W. Hansen, A. T. Delariva, S. R. Challa and A. K. Datye, *Acc. Chem. Res.*, 2013, **46**, 1720–1730.

8 S. J. Tauster, S. C. Fung and R. L. Garten, *J. Am. Chem. Soc.*, 1978, **100**, 170–175.

9 B. R. Powell and S. E. Whittington, *J. Catal.*, 1983, **81**, 382–393.

10 C. J. Pan, M. C. Tsai, W. N. Su, J. Rick, N. G. Akalework, A. K. Agegnehu, S. Y. Cheng and B. J. Hwang, *J. Taiwan Inst. Chem. Eng.*, 2017, **74**, 154–186.

11 J. Panpranot, K. Phandinthong, T. Sirikajorn, M. Arai and P. Praserthdam, *J. Mol. Catal. A Chem.*, 2007, **261**, 29–35.

12 Q. Fu and T. Wagner, *Surf. Sci. Rep.*, 2007, **62**, 431–498.

13 R. Anton, *Thin Solid Films*, 1984, **120**, 293–311.

14 S. Kunwar, P. Pandey, M. Sui, Q. Zhang, M. Y. Li and J. Lee, *Nanoscale Res. Lett.*, 2017, **12**, 364–378.

15 T. Karakouz, A. B. Tesler, T. Sannomiya, Y. Feldman, A. Vaskevich and I. Rubinstein, *Phys. Chem. Chem. Phys.*, 2013, **15**, 4656–65.

16 J. M. Harrisp, R. Pretorius and Nicole, *Solid-State Electrotronics*, 1978, **21**, 667–675.

17 E. Saiz, a. P. Tomsia and R. M. Cannon, *Acta Mater.*, 1998, **46**, 2349–2361.

18 F. Pesty, H. P. Steinrück and T. E. Madey, *Surf. Sci.*, 1995, **339**, 83–95.

19 W. Juszczyk, D. Łomot, J. Pielaszek and Z. Karpi, 2002, **78**, 95–98.

20 S. Helveg, I. Chorkendorff, M. Skoglundh, S. B. Simonsen and S. Dahl, *Surf. Sci.*, 2015, **648**, 278–283.

21 D. Levy, A. Grob, J. J. Grob and J. P. Ponpon, *Appl. Phys. A Solids Surfaces*, 1984, **35**, 141–144.

22 V. Ghetta and D. Chatain, *J. Am. Ceram. Soc.*, 2004, **85**, 961–964.

23 B. Schleich, D. Schmeisser and W. Göpel, *Surf. Sci.*, 1987, **191**, 367–384.

24 M. Kracker, W. Wisniewski and C. Rüssel, *RSC Adv.*, 2014, **4**, 48135–48143.

25 R. S. Goeke and A. K. Datye, *Top. Catal.*, 2007, **46**, 3–9.

26 S. Q. Wang, *MRS Bull.*, 1994, **19**, 30–40.

27 J. D. McBrayer, *J. Electrochem. Soc.*, 1986, **133**, 1242.

28 L. C. A. van den Oetelaar, R. J. A. van den Oetelaar, A. Partridge, C. F. J. Flipse and H. H. Brongersma, *Appl. Phys. Lett.*, 1999, **74**, 2954–2956.

29 A. A. Gosavi, J. L. Hedrick, P.-C. Chen, J. M. Notestein and C. A. Mirkin, *Nano Res.*, 2019, **12**, 1223–1228.

30 L. J. de Vreede, M. Schmidt Muniz, A. Van Den Berg and J. C. T. Eijkel, *J. Micromechanics Microengineering*, 2016, **26**, 37001–37006.

31 L. J. de Vreede, A. Van Den Berg and J. C. T. Eijkel, *Nano Lett.*, 2015, **15**, 727–731.

32 L. K. Ono, F. Behafarid and B. R. Cuenya, *ACS Nano*, 2013, **7**, 10327–10334.

33 T. Park, S. J. Lee, J. H. Cha and W. Choi, *Nanoscale*, 2018, **10**, 22623–22634.

34 K. Kirchhoff, M. Odijk, H. Le-The, A. van den Berg, M. Kappl, M. Müller, D. Lohse, J. C. T. Eijkel and C. Tregouet, *Nanotechnology*, 2018, **30**, 065301.

35 S. Kwon, S. Jang, J. W. Choi, S. Choi, S. Jang, T. W. Kim and G. Wang, *Nano Lett.*, 2017, **17**, 7462–7470.

36 B. K. Min, A. K. Santra and D. W. Goodman, *Catal. Today*, 2003, **85**, 113–124.

37 W. Juszczyk, Z. Karpiński, D. Łomot and J. Pielaszek, *J. Catal.*, 2003, **220**, 299–308.

38 B. K. Min, A. K. Santra and D. W. Goodman, *J. Vac. Sci. Technol. B Microelectron. Nanom. Struct.*, 2003, **21**, 2319.

39 J. P. Spatz, S. Mößmer and M. Möller, *Chem. - A Eur. J.*, 1996, **2**, 1552–1555.

40 D. Pan, Q. Fu and J. Lu, *Nanotechnology*, 2012, **23**, 305302.

41 J. P. Spatz, A. Roescher and M. Moller, *Adv. Mater.*, 1996, **8**, 337–340.

42 J. Shen, D. Zhang, F. Zhang and Y. Gan, *Appl. Surf. Sci.*, 2017, **422**, 482–491.

43 G. Meng, T. Yanagida, M. Kanai, M. Suzuki, K. Nagashima, B. Xu, F. Zhuge, A.

533 Klamchuen, Y. He, S. Rahong, S. Kai and T. Kawai, *Phys. Rev. E - Stat. Nonlinear, Soft*
534 *Matter Phys.*, , DOI:10.1103/PhysRevE.87.012405.
535 44 E. Saiz, A. P. Tomsia and R. M. Cannon, *Scr. Mater.*, 2001, **44**, 159–164.
536 45 M. Sui, P. Pandey, M. Y. Li, Q. Zhang, S. Kunwar and J. Lee, *Appl. Surf. Sci.*, 2017, **393**,
537 23–29.
538 46 P. M. Ajayan and L. D. Makrs, *Nature*, 1989, **338**, 139–141.
539 47 Q. Xu, K. C. Kharas, B. J. Croley and A. K. Datye, *ChemCatChem*, 2011, **3**, 1004–1014.
540 48 S. E. Wanke and P. C. Flynn, , DOI:10.1080/01614947508067523.
541 49 D. W., T. M. and S. B.H., *Adv. Funct. Mater.*, 2003, **13**, 61–65.
542 50 Y. Kojima and T. Kato, *Nanotechnology*, , DOI:10.1088/0957-4484/19/25/255605.
543 51 S. T. Han, Y. Zhou, Z. X. Xu, L. B. Huang, X. B. Yang and V. A. L. Roy, *Adv. Mater.*,
544 2012, 24, 3556–3561.
545 52 I. Sevonkaev, V. Privman and D. Goia, *J. Solid State Electrochem.*, 2013, **17**, 279–297.
546
547

548

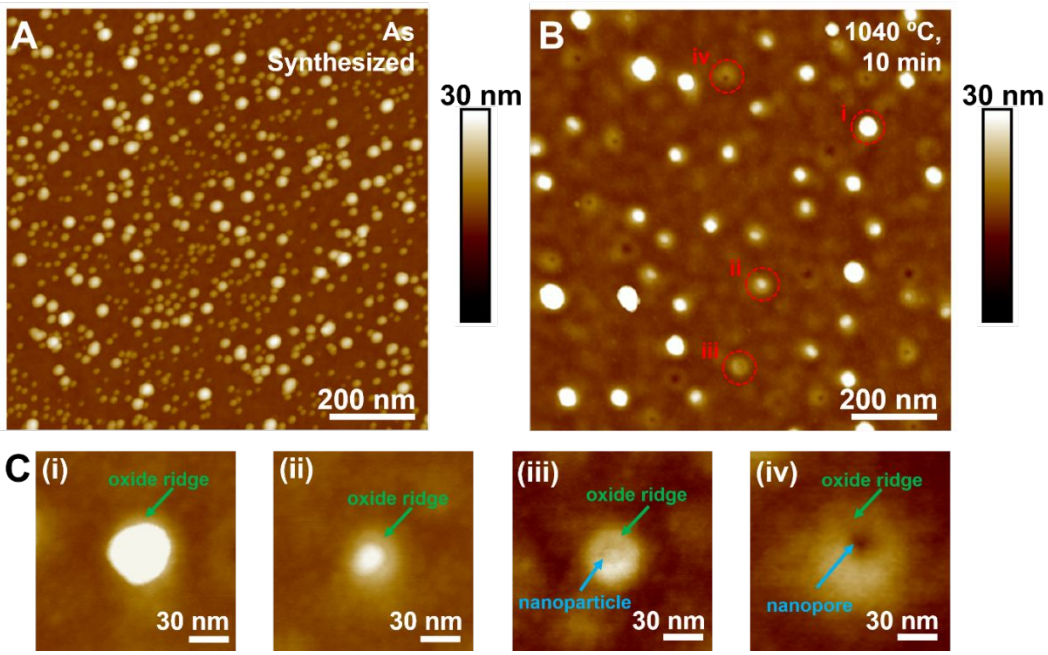

549

550 **Figure 1** AFM images of Pd nanoparticles on a Si-SiO_2 (285 nm) surface A) as synthesized by block
551 copolymer micelle lithography followed by annealing at 150 ºC (Ar) and 500 ºC (H_2) for 10 h each and B)
552 after RTP at 1040 ºC for 10 min using a ramp rate of 3.3 ºC/s. C) Pd nanoparticles at different stages of
553 thermal entrenchment after RTP showing i) agglomeration with low oxide ridge formation and without
554 entrenchment, ii) partial entrenchment with oxide ridge formation, iii) near-complete entrenchment with
555 oxide ridge formation, and iv) complete entrenchment (nanopore formation) with oxide ridge formation.

556

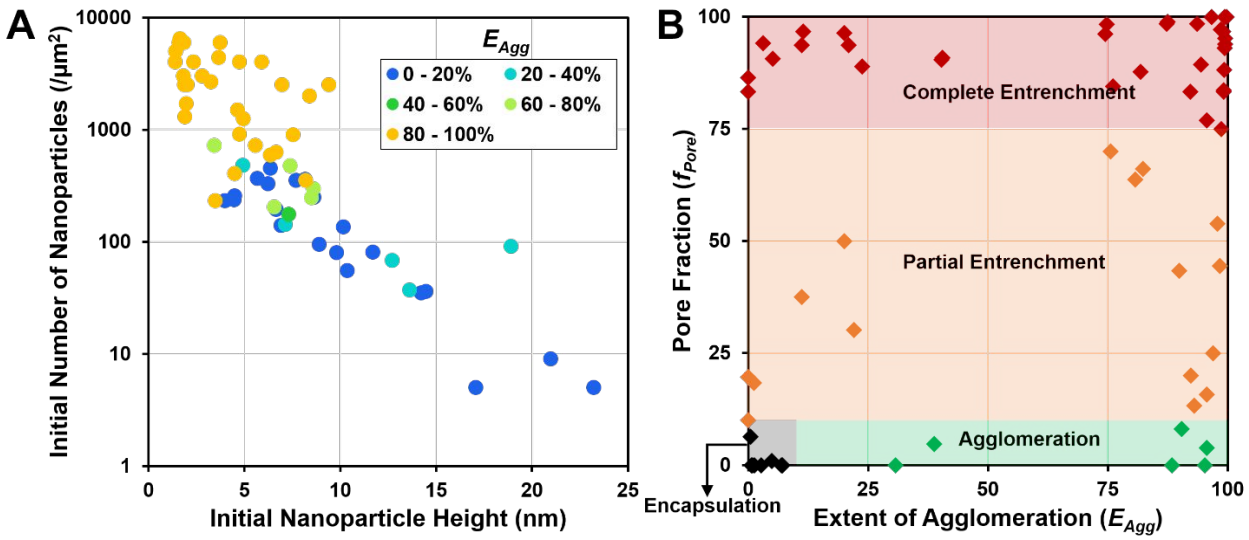

557

558 **Figure 2** A) Tendency to agglomerate (with or without nanopore formation) across different initial
559 nanoparticle distributions after RTP at 1040 ºC for 10 min using a ramp rate of 3.3 ºC/s. B) Defining different
560 behaviors based on observed pore fraction (f_{Pore}) and extent of agglomeration (E_{Agg}) after RTP.

561

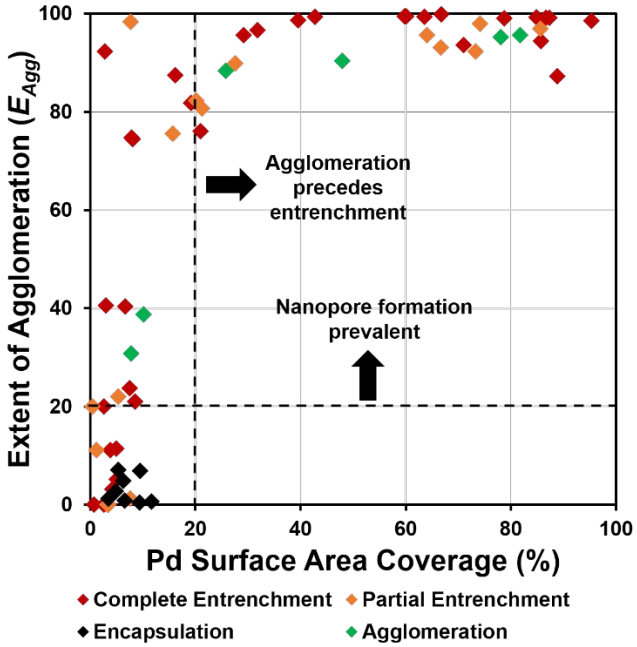

562

563 **Figure 3** Behaviors (complete and partial entrenchment, encapsulation, and agglomeration) observed as a
564 function of Pd surface area coverage and E_{Agg} of Pd/SiO_2 after RTP at 1040 ºC for 10 min using a ramp
565 rate of 3.3 ºC/s.

566

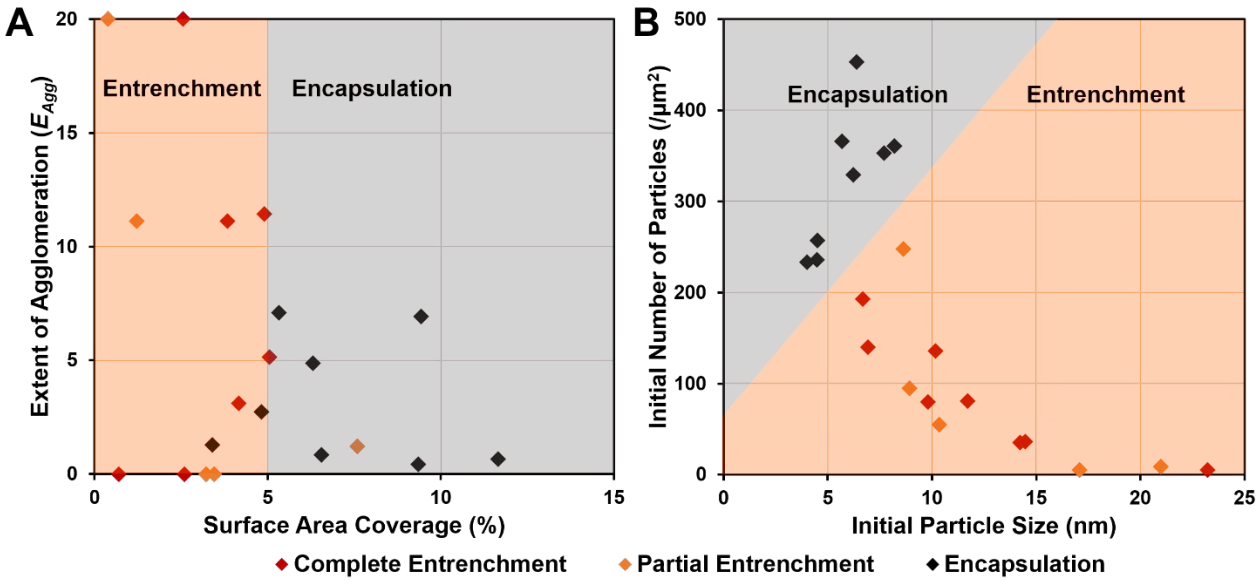

Figure 4 Pd/SiO_2 distributions after RTP at 1040 ºC for 10 min using a ramp rate of 3.3 ºC/s that result in minimal aggregation (E_{Agg} < 20 %) have surface area coverages less than 15 %. A) In this range, entrenchment, complete or partial, is dominant up to 5% surface area coverage whereas encapsulation is dominant between 5 – 15% coverages. B) Alternately plotted, encapsulation is dominant for smaller nanoparticles sizes (4 – 8 nm) and intermediate surface densities (200 – 500 nanoparticles /μm²), while entrenchment is dominant at larger nanoparticle sizes (6 – 25 nm) and lower surface densities (10 – 250 nanoparticles /μm²). Higher densities of small nanoparticles (not shown) agglomerate, then entrench.

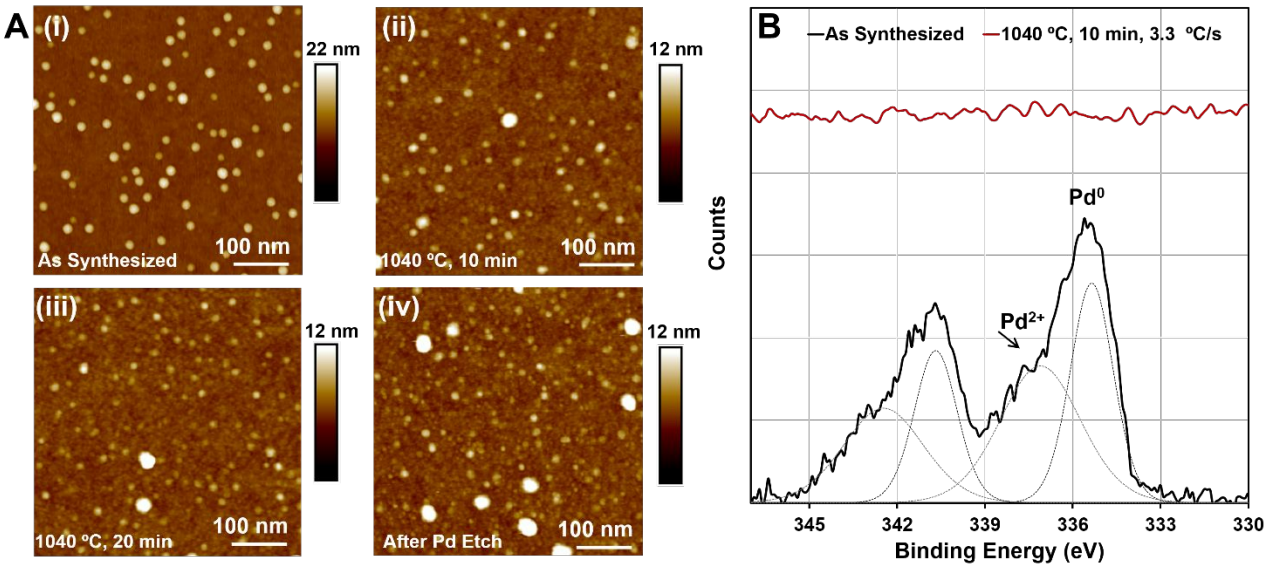

Figure 5 A) AFM images of a Pd/SiO_2 surface i) as synthesized, ii) after RTP at 1040 ºC for 10 min using a ramp rate of 3.3 ºC/s, iii) after heating the surface in ii for an additional 10 min, and iv) after Pd etching of the surface in iii. B) Surfaces that show encapsulation lose their Pd XPS features after RTP at 1040 ºC for 10 min using a ramp rate of 3.3 ºC/s.

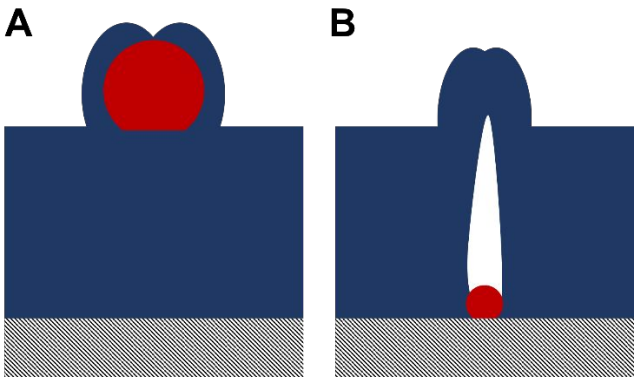

582

583 **Scheme 1** Proposed mechanism of Pd nanoparticle encapsulation within the SiO_2 support by: A)
584 nanoparticle encapsulation by oxide ridges before nanopore formation, and B) closing of the nanopores by
585 large oxide ridges after entrenchment.

586

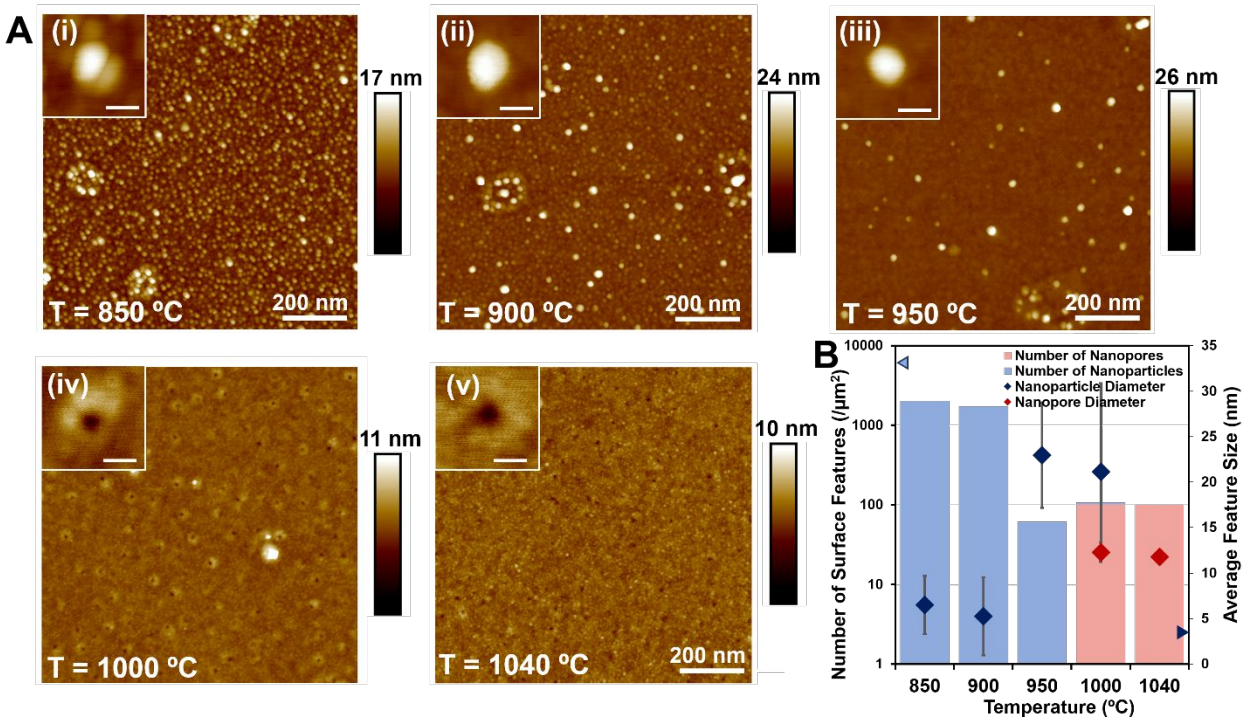

Figure 6 A) AFM images of an initially high surface density of small Pd nanoparticles on SiO_2 following RTP using a ramp rate of 3.3 °C/s and held for 10 min at i) 850, ii) 900, iii) 950, iv) 1000, and v) 1040 °C. B) Trends in nanoparticle and nanopore surface densities and sizes at each temperature. All inset scale bars are 20 nm. The nanoparticle surface density and diameter before heating are indicated by the arrowheads on each axis.

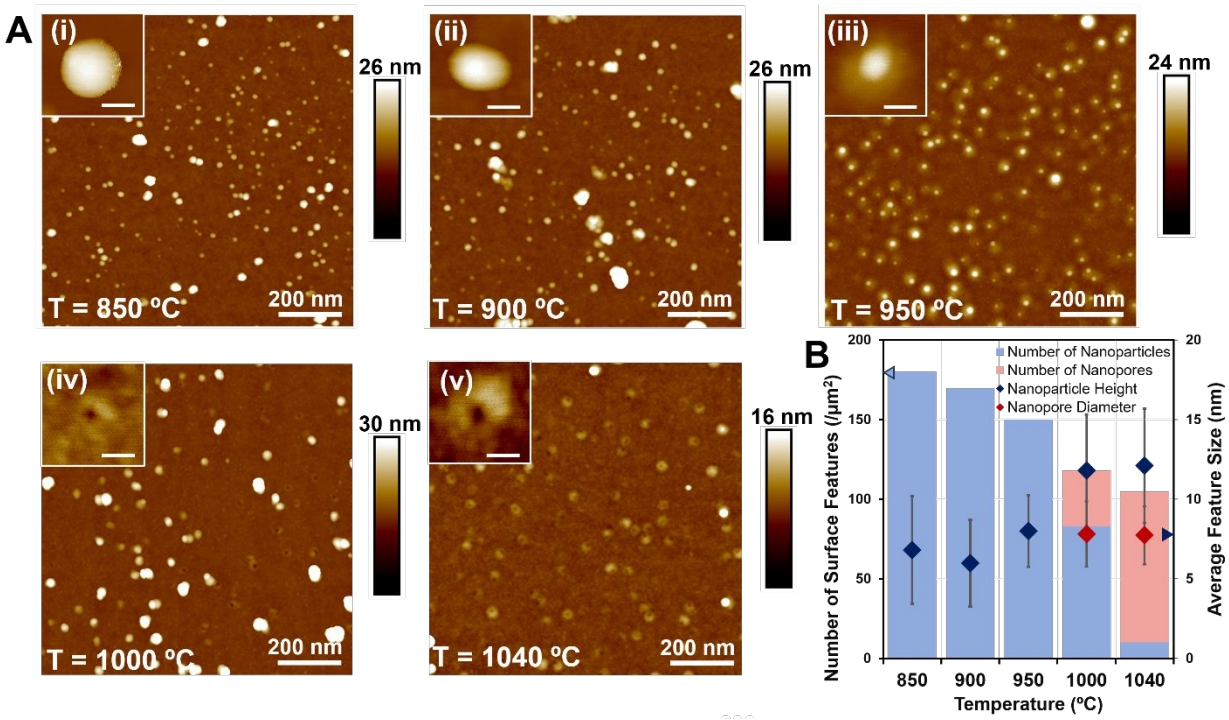

Figure 7 A) AFM images of an initially low surface density of large Pd nanoparticles on SiO_2 following RTP using a ramp rate of 3.3 °C/s and held for 10 min at i) 850, ii) 900, iii) 950, iv) 1000, and v) 1040 °C. B) Trends in nanoparticle and nanopore surface densities and sizes at each temperature. All inset scale bars are 20 nm. The nanoparticle surface density and height before heating are indicated by the arrowheads on each axis.

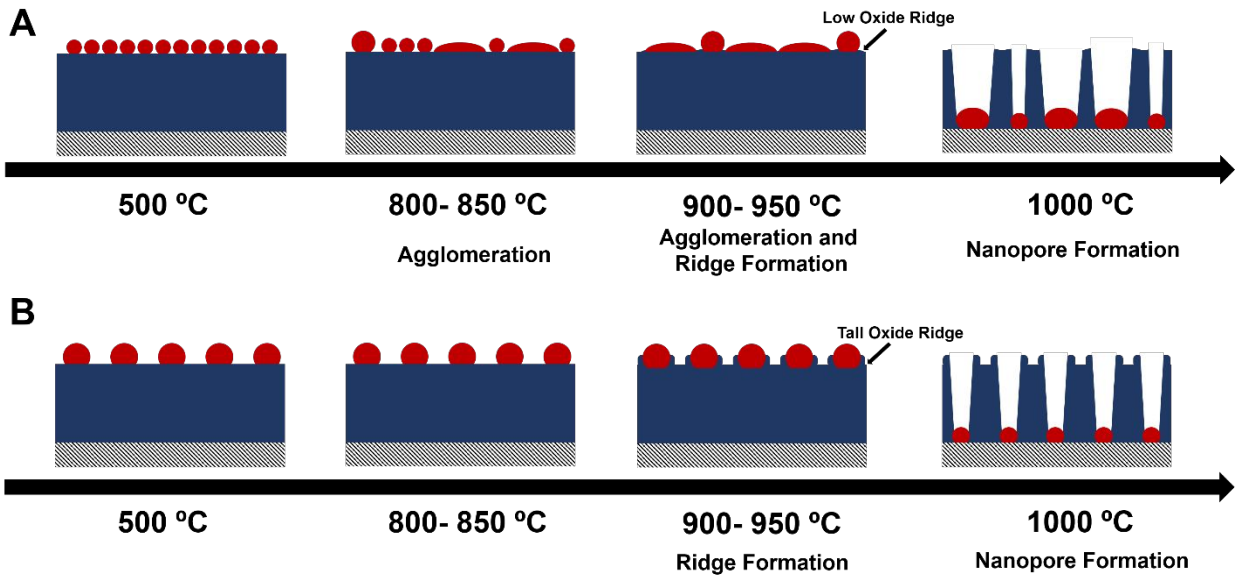

601

602 **Scheme 2** Proposed behaviors of A) high density of small Pd nanoparticles, and B) low surface density of

603 large Pd nanoparticles at increasing RTP hold temperatures.

604

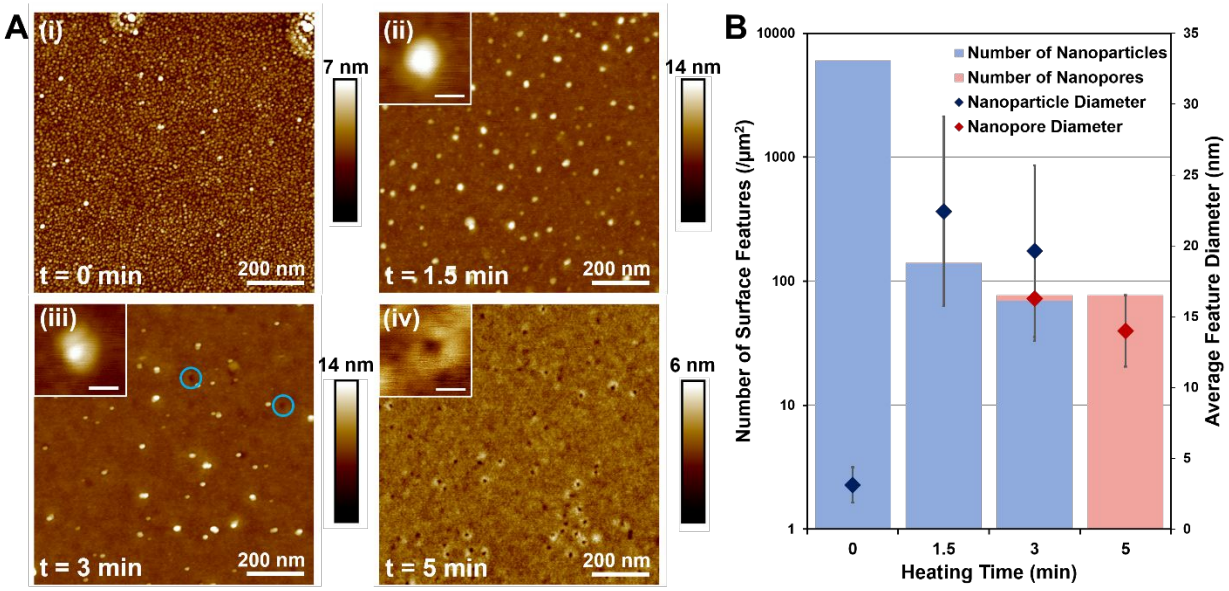

Figure 8 A) AFM images of i) an initially high surface density of small Pd nanoparticles on SiO_2 and ii) following RTP with ramp of 3.3 ºC/s to 1040 ºC for 1.5 min, iii) 3 min, and iv) 5 min. B) Trends in nanoparticle and nanopore surface densities and diameters at each time point. All inset scale bars are 20 nm.

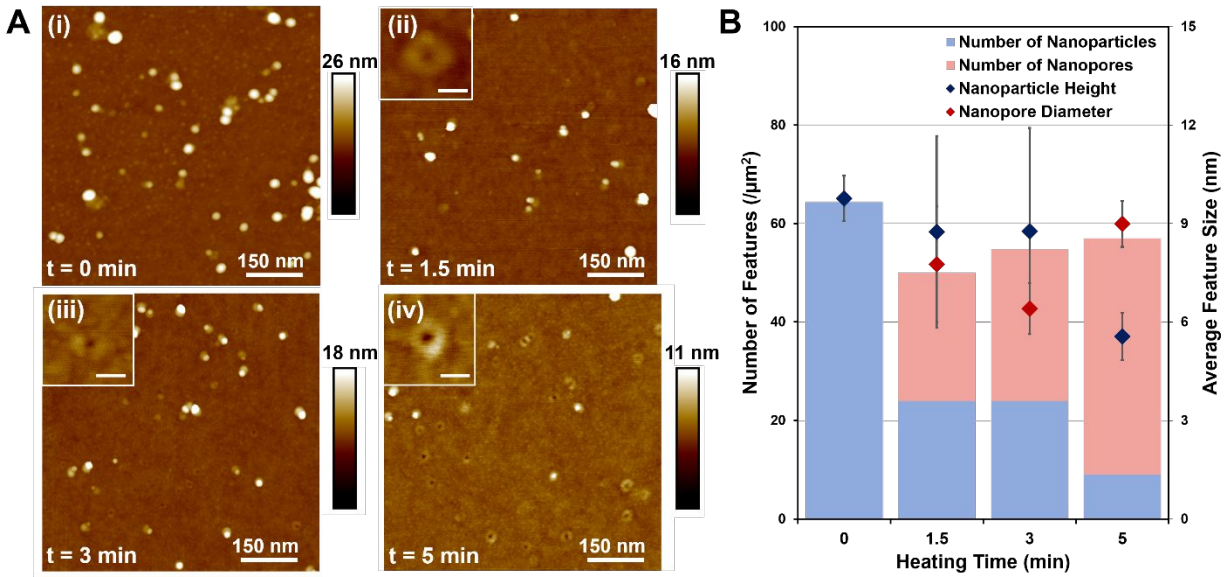

610

611 **Figure 9** A) AFM images of i) an initially low surface density of large Pd nanoparticles on SiO_2 and ii)
612 following RTP with a ramp of at 3.3 ºC/s to 1040 ºC for 1.5 min, iii) 3 min, and iv) 5 min. B) Trends in
613 nanoparticle and nanopore surface densities and sizes at each time point. All inset scale bars are 20 nm.

614

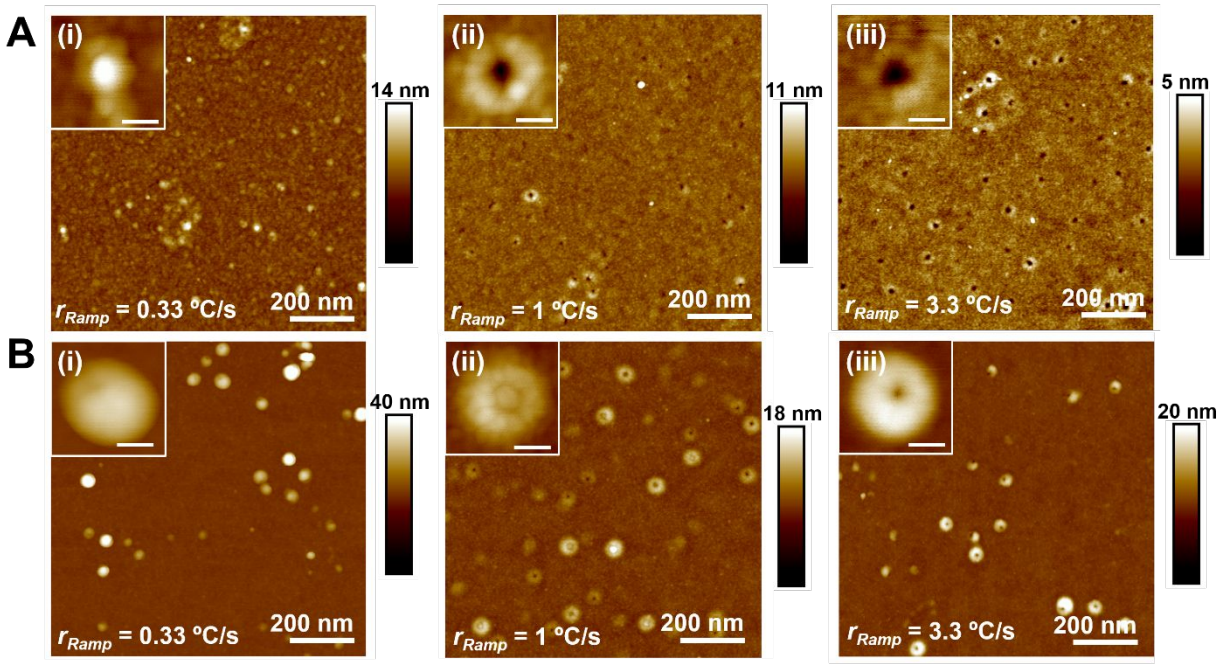

Figure 10 AFM images of A) an initially high surface density of small Pd nanoparticles on SiO_2 following RTP with a 10 min hold at 1040 ºC and ramp rates (r_{Ramp}) of i) 0.33, ii) 1, and iii) 3.3 ºC/s and B) an initially low surface density of large Pd nanoparticles on SiO_2 following RTP with a 10m in hold at 1040 ºC and ramp rates of i) 0.33, ii) 1, and iii) 3.3 ºC/s

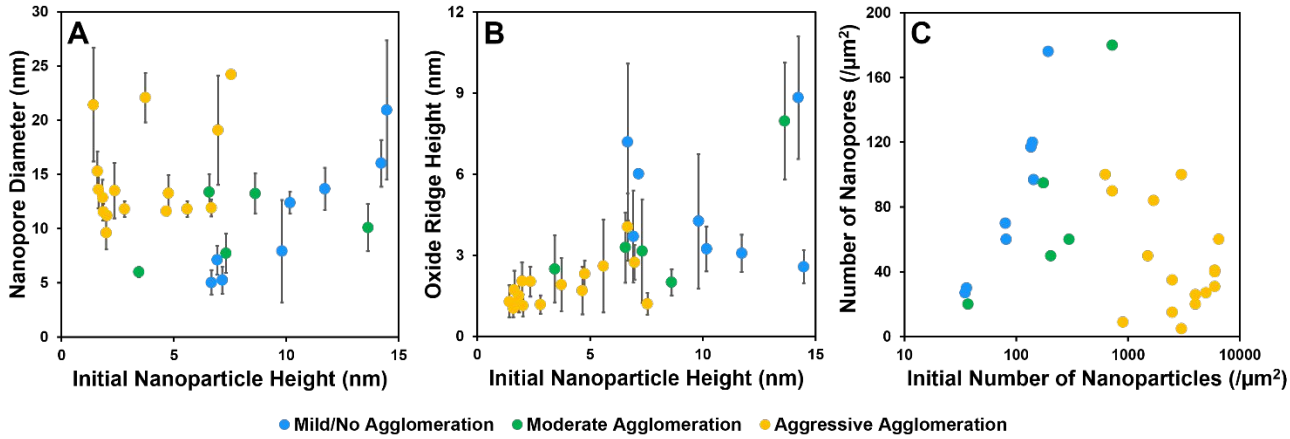

621

622 **Figure 11** A) Average nanopore diameter as a function of initial nanoparticle height, B) average oxide ridge
623 height as a function of initial nanoparticle height, and C) number density of nanopores formed as a function
624 of initial number density of Pd nanoparticles. The different extents of agglomeration are also shown. Mild/no
625 agglomeration (E_{Agg} < 20 %), Moderate agglomeration (20% < E_{Agg} < 80 %), and Extreme agglomeration
626 (E_{Agg} > 80 %).

627

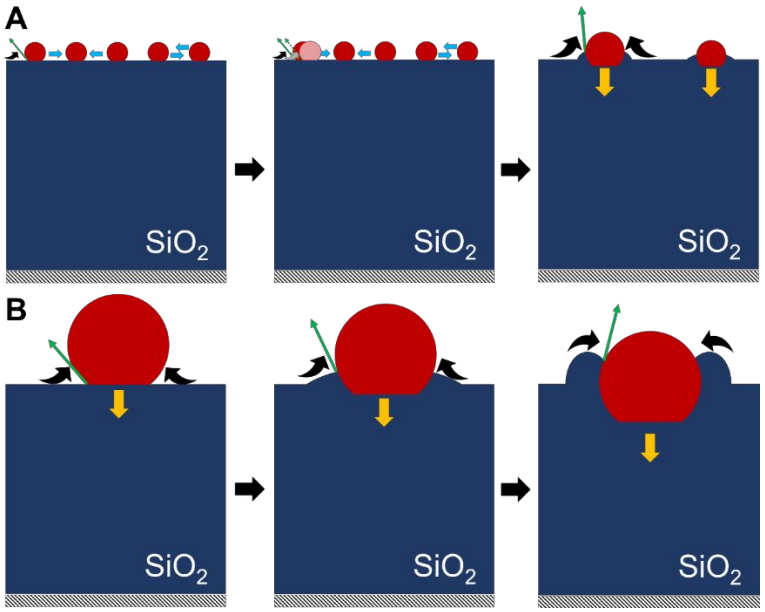

628

629 **Scheme 3** Proposed temporal evolution of oxide ridges when samples are held above 1000 ºC for an initial

630 A) high density of small Pd nanoparticles, and B) low density of large Pd nanoparticles.

Mapping the thermal entrenchment behavior of Pd nanoparticles on planar SiO_2 supports

Abha Gosavi[#, ‡], Chad Mirkin[#, ‡, §, ψ, *], Justin Notestein[#, *]

[#]Department of Chemical and Biological Engineering, [‡]International Institute for Nanotechnology, [§]Department of Chemistry, and [ψ]Department of Materials Science and Engineering, Northwestern University, 2145 Sheridan Road, Evanston, Illinois 60208, United States

**chadnano@northwestern.edu, j-notestein@northwestern.edu*

Table of Contents Image